**50th AIAA/ASME/ASCE/AHS/ASC Structures, Structural Dynamics, and Materials Conference
17th**
4 - 7 May 2009, Palm Springs, California

AIAA 2009-2416

Videogrammetry Dynamics Measurements of a Lightweight Flexible Wing in a Wind Tunnel

Nathan A. Pitcher[1]
Air Force Research Laboratory, Wright-Patterson AFB, Ohio, 45433

Jonathan T. Black[2], Mark F. Reeder[3], and Raymond C. Maple[4]
Air Force Institute of Technology, Wright Patterson AFB, Ohio, 45433

Videogrammetry is a measurement technique well-suited to characterizing lightweight, flexible wings in wind tunnel testing. It is non-contact, full-field, and can capture the large amplitude deflections experienced by the wings. Here videogrammetry is used to analyze the spectral content of the motion of a flexible Nighthawk mini-UAV wing and animate the operating deflection shapes of the wing corresponding to structural resonance frequencies. The wing was tested at angles of attack ranging from -5° to 13°, and wind speeds ranging from 20 to 40 mph. Results show the flexible wing tends to experience flapping behavior at low angles of attack. This behavior is confirmed by the spectral content of the wing displacements and the corresponding animated deflection shapes. This type of video-grammetry extends standard videogrammety techniques to the spectral analysis and visualization of resonance shapes. The data is necessary to validate numerical models of the wings, understand complicated membrane-structure interactions, and optimize wing performance in different flight regimes.

I. Introduction

UNMANNED Aerial Vehicles (UAVs) are aircraft with a host of potential military and civilian applications. The size of current UAVs varies widely with wingspans ranging from approximately 18 cm to 40 m. Mini-UAVs – defined here as having wingspans ranging from 0.5 to 3.5 meters – currently in the field are predominately used for surveillance and reconnaissance. The Nighthawk mini-UAV shown in Fig. 1 was designed for aerial surveillance. It has a removable 66 cm span wing that can be stored in-line with the aircraft, carries forward and side facing cameras and a side facing thermal imager, weighs 0.68 kg (1.5 lbs), and flies at wind speeds of 18–40 knots (30–75 km/h). It exploits GPS and autopilot technology for navigation, has a loiter time of 70–90 minutes, and a range of 2–10 km.

Videogrammetry is the science of making time history measurements from synchronized videos from multiple cameras imaging the same object. Previous efforts to measure wing deformation and twist in wind tunnels have used videogrammetry and its static counterpart photogrammetry.[1-3] Videogrammetry has also been used to measure resonance frequencies of aeroelastic models.[4] Three-dimensional surface measurements of static deflected shape and strain in wind tunnels have been taken using both multi-camera videogrammetry and projection moiré interferometry.[5-7] These studies found significant billowing, bending, and washout occurring in lightweight and flexible wings, making these kinds of image-based measurements valuable tools.

---

[1] Capt, Research Engineer, Computational Sciences Branch, AFRL/RBAC, 2210 8th St, Bldg 146, AIAA Member.

[2] Assistant Professor, Department of Aeronautics and Astronautics, 2950 Hobson Way, AIAA Member.

[3] Associate Professor, Department of Aeronautics and Astronautics, 2950 Hobson Way, AIAA Member.

[4] Former Assistant Professor, currently with Hawker Beechcraft Inc, Wichita, KS, AIAA Senior Member.

The views expressed in this paper are those of the authors and do not reflect the official policy or position of the United States Air Force, Department of Defense, or the U.S. Government.
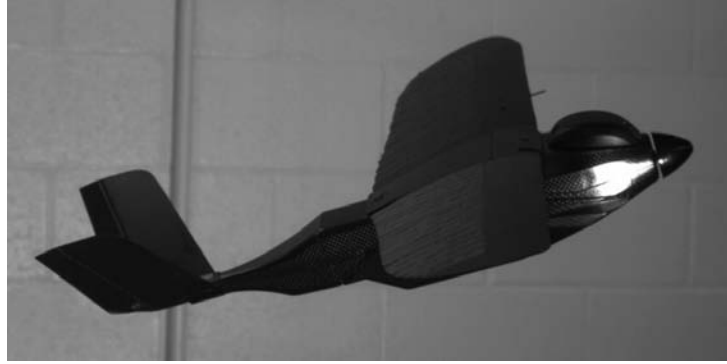
Fig. 1 Nighthawk mini-UAV.

Videogrammetry has also been used to measure both the resonance frequencies and corresponding operating deflection shapes (ODS) of large lightweight flexible membrane-based space structures. Again, this measurement technology is well-suited to such challenging structures because it is non-contact and therefore does not change the mass or stiffness of the object being measured, and captures low-frequency large-amplitude motion.[8-10] As mini-UAV and micro air vehicle (MAV) development trend toward lighter, membrane-based, and even flapping wings, such experimental techniques can provide valuable data.

The purpose of this study is to use non-contact videogrammetry measurement techniques to characterize dynamic behavior of flexible, lightweight mini-UAV wings undergoing wind tunnel tests. It will extend previous non-contact videogrammetry measurement techniques to the measurement of the resonance frequencies and corresponding ODSs of the Nighthawk wings. Knowledge of the deflection shape of the wing at different resonance frequencies is necessary to validate structural, aeroelastic, and aerodynamic numerical models, optimize wing aerodynamic performance as a function of angle of attack (AoA), Reynolds number (*Re*), and geometry, and control flutter. Previous efforts to characterize the performance of the Nighthawk mini-UAV measured the static wing deflection at various AoAs to analyze the lift, drag, and pressure distributions through computation fluid dynamics (CFD).[11-13]

II. Test Setup

A production model Nighthawk was provided by Applied Research Associates for wind tunnel testing. The model has no internal components other than the motor for the propeller on which the nose spinner is mounted. It is 51 cm long with a 66 cm wingspan. The Nighthawk's body is composed of a carbon fiber composite. The leading edge of the lightweight and flexible wing and the wing ribs are also made of carbon fiber, while the gaps between the ribs are spanned by nylon cloth. The root chord is 15.25 cm and the wing has an elliptic planform. The root camber of the undeflected wing is approximately 7.8%. The incidence angle is approximately 4.8^o and the dihedral of the undeflected wing is approximately 4.9^o. The planform area of the wing is 0.0457 m^2 and the Aspect Ratio (AR) is 4.8. Typical Reynolds numbers range from 90,000 to 180,000.

Flexible wings offer several advantages over rigid wings. Smoother flight and greater stall resistance at high AoAs are both products of adaptive washout. Adaptive washout occurs when a flexible wing deforms due to the aerodynamic loads experienced during flight. At high AoA's or increased airspeed, the wing will decamber and twist forward reducing the apparent AoA at the wing tip, providing increased stall resistance and improved gust response. Another advantage of a flexible wing is increased roll stability. The wing tips of a flexible wing aircraft will deflect upwards during flight due to the lift on the wings, increasing dihedral and resulting in greater roll stability.[14,15] Studies on rigid and flexible versions wings of the same geometry as tested here confirm that the flexible wings showed increased stability in roll, pitch, and yaw, improved efficiency in the form of a higher lift to drag ratio, improved portability, and found that washout in the flexible wing can delay the onset of stall.[16]

Three significant changes were made to the Nighthawk before testing began. The mini-UAV was fitted with an internal mounting block, the upper wing surface was marked with high contrast targets for videogrammetry measurement, and the propeller blades were removed to compare more closely with the CFD model. The ruddervators were free throughout all tests.

Two types of high-contrast targets were attached the upper wing surface: non-coded targets (circular dots) and coded targets (circular dots surrounded by banded sections). The non-coded targets are bright yellow circles 0.635 cm in diameter. This size was selected to ensure the diameters were at least 8-10 pixels in photographs, which is

ideal for automatic target recognition during image processing. The coded targets are automatically recognized by the processing software and are used to orient the photos (cameras).
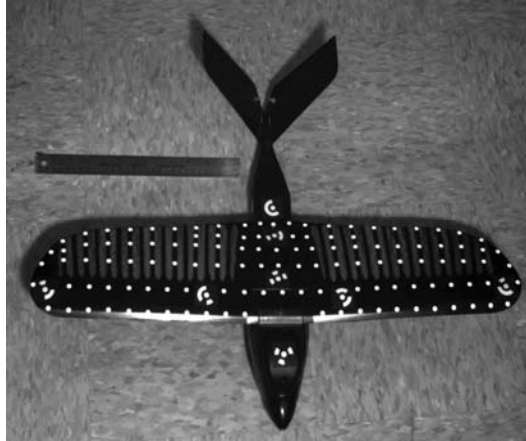

Fig. 2 Nighthawk mini-UAV wing marked for videogrammetry.

All attached targets were low profile to minimize their impact on airflow over the wing. Targets were only attached to the carbon fiber composite leading edge and ribs to avoid altering the mass and stiffness of the nylon cloth. The targets were positioned on the wing in rows spaced approximately 2.5 cm apart with the first row starting 1.25 cm behind the leading edge. This spacing ensured easy sorting of the targets during post processing. Fig. 2 shows the Nighthawk after it was marked with targets.

Testing was conducted in the low speed open circuit wind tunnel at the Air Force Institute of Technology (AFIT), shown in Fig. 3. The test section is 1.12 m wide, 0.79 m high, and 1.83 m long. Maximum airspeed in the test section is 240 km/h. There are windows on the ceiling and on each side of the test section, and is has a white floor, which contrasts well with the black wing of the Nighthawk. However, at moderate speeds and AoAs, washout occurred and the targets near the leading edge of the wing blended into the wind tunnel floor when viewed from above. To provide contrast for the targets on the leading edge, black felt was attached to the floor of the wind tunnel, ensuring target recognition despite washout.
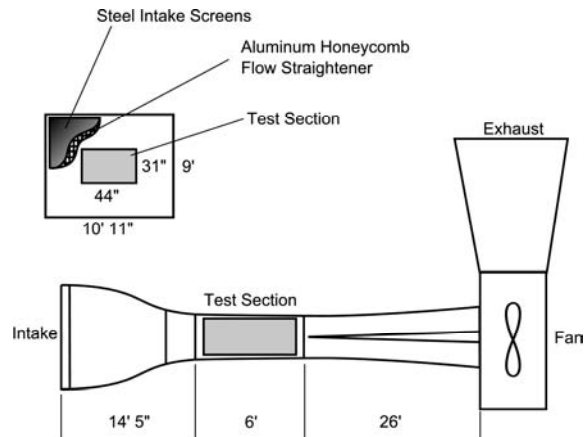

Fig. 3 AFIT wind tunnel schematic.[16]

Six coded targets were secured to the wind tunnel floor to act as reference points during post processing (Fig. 4). These targets were visible in each camera. Targets 1 and 2 define the x-axis (positive from 2 to 1) and the scaling factor since they are separated by 47.1 cm. Targets 2 and 3 define the y-axis (positive from 2 to 3). The z-axis is normal to the wind tunnel floor (up is positive).
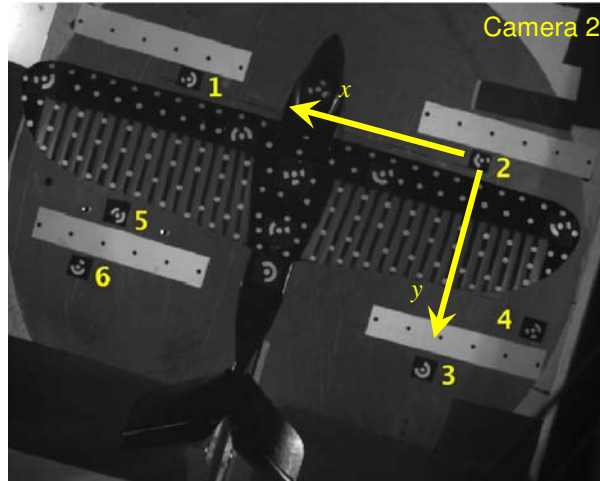
American Institute of Aeronautics and Astronautics

Fig. 4 Image from videogrammetry Camera 2 used in processing.

At AoAs less than 4°, the targets on the wing lie in a plane approximately 38 cm above the wind tunnel floor. The only targets out of this plane were the coded targets used to define the scale and axes. Due to the 3D nature of the videogrammetry process, difficulty can occur when measuring planar objects due to a lack of information about the out-of-plane dimension. Non-coded targets were therefore added to the wind tunnel floor (Fig. 4) to maintain accuracy and aid in solution convergence by providing out-of-plane measurement points.

Three synchronized Basler 501k high speed digital cameras captured image sequences during wind tunnel testing. Each camera is capable of capturing a maximum 75 frames per second (fps) at maximum resolution of 1280 x 1024 pixels. A custom computer workstation was used to drive the cameras and store image sequences. Each camera was connected to its respective video capture board in the PC. Image capturing software controlled the cameras via their respective video capture boards.

For optimal view of the wing, all cameras were positioned atop the wind tunnel and aimed through the viewing glass above the test section (Fig. 5). They were positioned in-line with the flow direction with Camera 1 in front of the Nighthawk, Camera 2 directly above the Nighthawk, and Camera 3 trailing the Nighthawk. There was at least a 30° separation angle between the cameras. The cameras were positioned far enough from the model to allow each camera a full view of the wing. Fig. 5 illustrates the viewing angle of each camera.
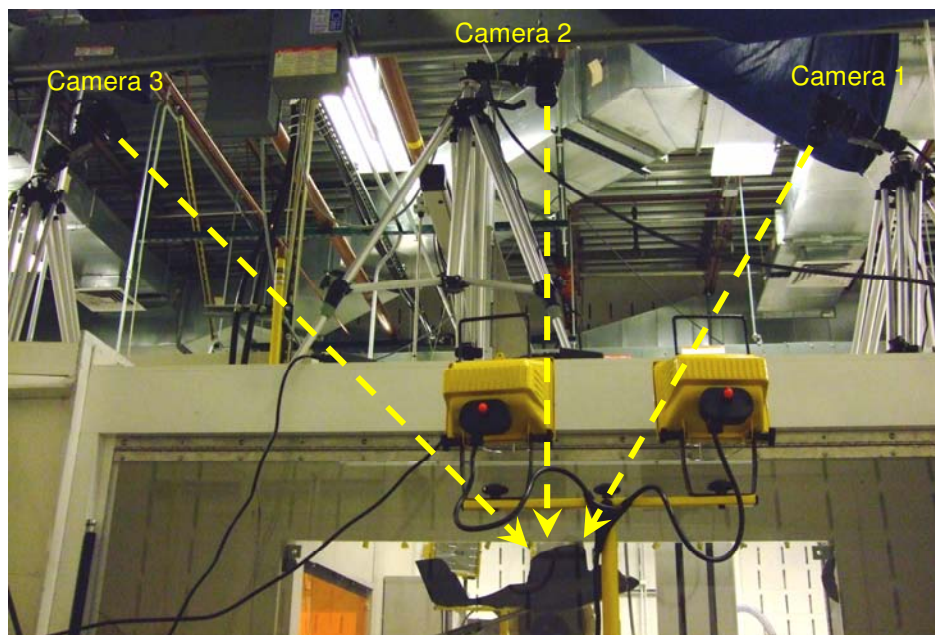

Fig. 5 Videogrammetry camera setup above wind tunnel imaging Nighthawk mini-UAV.

To provide accurate 3D data in time, it was important to ensure the cameras were synchronized. The first camera was configured as the master and the other two were slaves. A synchronization test was performed in which the captured image size was reduced to 480 pixels x 480 pixels to increase the frame rate to 156 fps. The collected image sequences were examined to verify the cameras imaged synchronously to substantially greater than the frame rate. Note the wind tunnel tests performed here were recorded at 75 fps.

Each of the three cameras was calibrated to remove image distortions caused by camera aberrations. This process calculates the focal length (zoom), location of the principal point, radial lens distortion, and decentering lens distortion of each camera, enabling accurate photographic measurements by compensating for any deviation of the recorded image from what would have been recorded by an ideal pin-hole camera.

Following calibration, a test was performed to ensure the wind tunnel glass did not distort the images and decrease measurement accuracy. This test involved capturing image sets of a precisely-machined calibration slate. The calibration slate is a black with small white targets in a grid measuring 135 mm x 80 mm. It is not typically used for camera calibration, however, because it has precisely located targets, it was useful in a test to determine the accuracy of the videogrammetry measurements. It was placed in the wind tunnel at about the same height as the wing. Image sets of the calibration slate were captured. The coded targets on the floor were used to scale the images, and the size of the calibration grid was measured using videogrammetry. Since the calibration slate is smaller than the wing, the test was performed several times with the calibration sheet moved to different positions covering the same field of view occupied by the wing. The maximum error measured in these tests was 0.62 mm. This error is acceptable since tip deflection is expected to be as high as 5 cm.

Proper lighting is paramount in capturing high quality images. The lighting was required to illuminate the high contrast targets without producing glare off the wing, the wind tunnel viewing glass, or the wind tunnel floor that may have washed-out targets or caused false targets.

AoA and wind speed were the independent variables during wind tunnel testing. Yaw angle and roll angle were control variables, held constant at 0°. The model was adjusted to the target AoA using the wind tunnel controller. The actual AoA of the Nighthawk was confirmed using an inclinometer for each angle tested. The tested AoA's were selected to correspond to lift coefficients (C_L) of slightly above 0.0 to slightly above 1.0. Here the AoA was measured from the flat bottom of the Nighthawk to wind tunnel horizontal as positioned on the sting. The geometry of the attachment of the wing to the fuselage creates the case in which -5° AoA corresponds to a C_L just greater than 0.0 and 13° AoA corresponds to a C_L just greater than 1.0 for all tested wind speeds.

In wind tunnel testing it is common to set the wind speed then perform a sweep of the AoAs while holding the velocity constant. The camera positioning allowed for only a 10° variation in AoA before targets would be lost from view. As a result, the velocities were varied at each AoA rather than performing an AoA sweep for each velocity. The cameras were positioned to accommodate testing for 3° to 13° AoA. Then the cameras were repositioned and tests were conducted for -5° to 3° AoA.

At each of the 10 AoA's at which the wings were tested a static image set of the wing was captured before the wind tunnel was activated to establish the undeflected wing position. The velocity was then increased to 20 mph and held constant for about 30 seconds until transients died out. Image sequences were then captured and the process was repeated for the 30 mph case and the 40 mph case. A second static (no-wind) image set was obtained after the 40 mph test was complete to compare with the first image set and ensure the wing returned to its original location (i.e. the wing or model didn't shift during the test).

Image sequences from the three synchronized cameras were captured at 75 fps for each of the 30 test cases listed in Table 1. A set of three simultaneous images, one from each camera, constitutes an image set, and the synchronized cameras produce one image set per frame. The 3D location of each target on the wing was triangulated for each image set through the following videogrammetry process: target centers were marked to subpixel accuracy on all three images; the software then traced rays in space from each camera to the marked targets; the 3D global location of the targets was determined by the intersection of rays from multiple cameras. A local coordinate system was specified using coded targets 1, 2, and 3 in Fig. 4. Once the first frame in the captured image sequence has been processed (i.e. the 3D location of each target has been solved), the targets can be tracked through the remaining frames. The location of each target in each frame can then be exported to a data file. The final result is a set of 3D target locations in time. This process is summarized in Fig. 6.
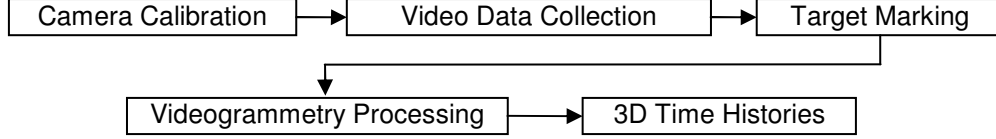
Fig. 6 Videogrammetry process.

The collinearity equations that trace rays from cameras to targets, relating the global 3D target location (X, Y, Z) to the corresponding point (x, y) in the image plane are:[1,17]

$$x - x_p - dx = -c \frac{m_{11}(X - X_c) + m_{12}(Y - Y_c) + m_{13}(Z - Z_c)}{m_{31}(X - X_c) + m_{32}(Y - Y_c) + m_{33}(Z - Z_c)}$$

(1)

$$y - y_p - dy = -c \frac{m_{21}(X - X_c) + m_{22}(Y - Y_c) + m_{23}(Z - Z_c)}{m_{31}(X - X_c) + m_{32}(Y - Y_c) + m_{33}(Z - Z_c)}$$

In Eq. (1), the parameter set (c, x_p, y_p) is the interior orientation of a camera calculated during camera calibration, where c is the principal distance of the lens, and x_p, and y_p are the principal-point coordinates on the image plane. ω, ϕ, κ, X_c, Y_c, Z_c define the global 3D orientation of a camera, where (ω, ϕ, κ) are the Euler rotational angles and (X_c, Y_c, Z_c) are the coordinates of the perspective global center. The coefficients m_{ij} $(i, j = 1, 2, 3)$ are the rotation matrix elements that are functions of (ω, ϕ, κ).[1,17]

More detail on photogrammetry and videogrammetry processing and measurements can be found in Refs 18–20.

American Institute of Aeronautics and Astronautics

Table 1 Test Matrix

AoA (deg)	Speed (mph)	Ambient Pressure (Torr)	Temp (^{o}F)	*Re*
-5.05	21.1	731.8	71.9	91317
	31.7	731.8	73.0	136942
	42.1	732.3	73.3	181857
-2.9	21.1	733.6	72.9	91375
	31.8	733.6	73.6	137529
	42.4	733.8	74.1	183280
-0.95	21.4	733.8	73.3	92656
	31.9	734.1	73.8	138003
	42.4	734.1	73.9	183410
1.15	21.1	734.3	73.5	91365
	31.8	734.3	73.9	137615
	42.6	734.3	74.1	184297
3.2	21.1	734.8	74.3	91293
	31.9	734.6	73.8	138121
	42.7	734.6	74.2	184763
5.1	21.7	744.7	69.4	96037
	32.3	744.7	69.4	142949
	43.1	744.5	68.8	190924
7.3	21.1	733.0	79.5	90192
	31.8	733.0	79.5	135929
	42.1	733.0	79.5	179957
9.4	21.5	732.5	80.7	91634
	32.2	732.3	81.2	137097
	42.1	732.3	82.0	178971
11.4	21.4	731.3	81.4	90951
	31.6	731.3	81.4	134302
	42.3	731.3	81.4	179777
13.4	21.4	731.3	81.8	90881
	31.5	731.3	81.8	133773
	42.1	731.3	81.8	178789

III. Results

The videogrammetry processing yielded sets of 3D point locations in time. The time history of one of these points is plotted in Fig. 7. This graph shows the out-of-plane *z*-position of a single point on the wing during one of the wind tunnel tests of the Nighthawk mini-UAV. The bottom graph of Fig. 7 shows the power spectral density (PSD) of that same point. In the frequency domain it is possible to see a resonance peak at approximately 31 Hz.
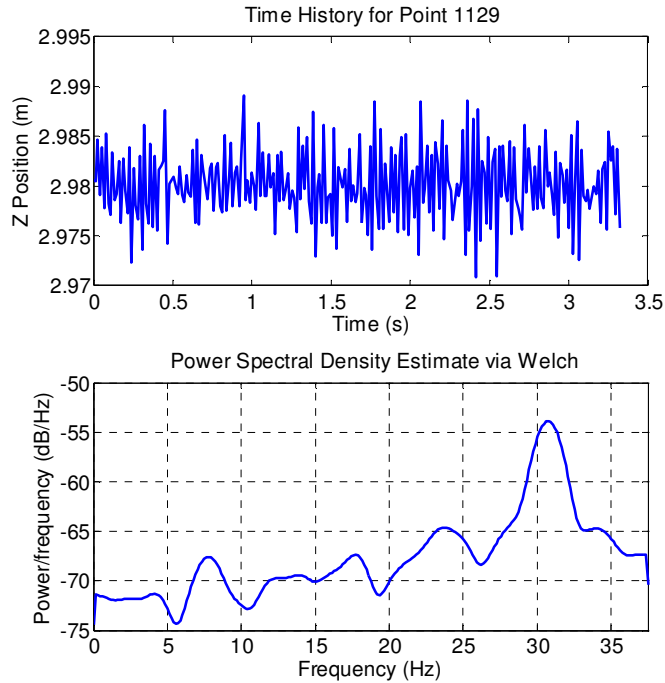
Fig. 7 Sample *z*-direction time history (top) and Power Spectral Density (bottom).

Standard practice is to use videogrammetry to measure the static deflection shape of the wing over the test.[5,7] This data can be plotted in several ways, including the average deflected shape from the undeflected no-wind condition, examples of which are shown in Fig. 8, the standard deviation of the vibration from the average deflected shape, shown in Fig. 9, and the maximum deflection from the average deflected shape, discussed later. The average deflected shapes in Fig. 8 shows that at low AoAs most of the deflection occurs at the trailing edge wing tip causing twist, while at higher AoAs the shapes involve more tip bending. The standard deviation from the average deflected shape in Fig. 9 shows larger amplitude vibrations occur as expected at the most flexible part of the wing, the trailing edge wing tip.
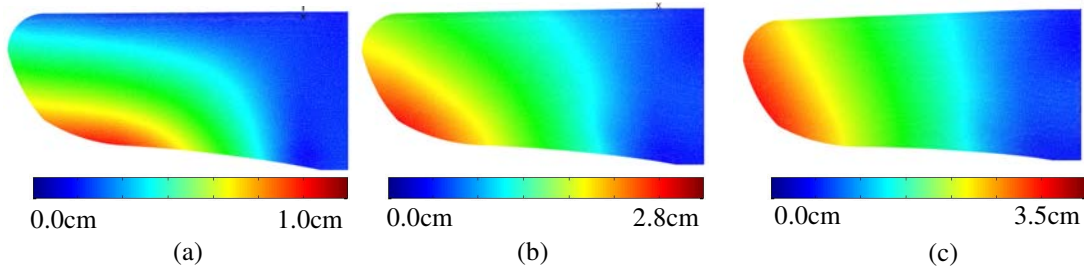

Fig. 8 Examples of average static deflected shapes of wing: (a) AoA -0.95°, Speed 30 mph, (b) AoA 5.1°, Speed 40 mph, (c) AoA 11.4°, Speed 40 mph.
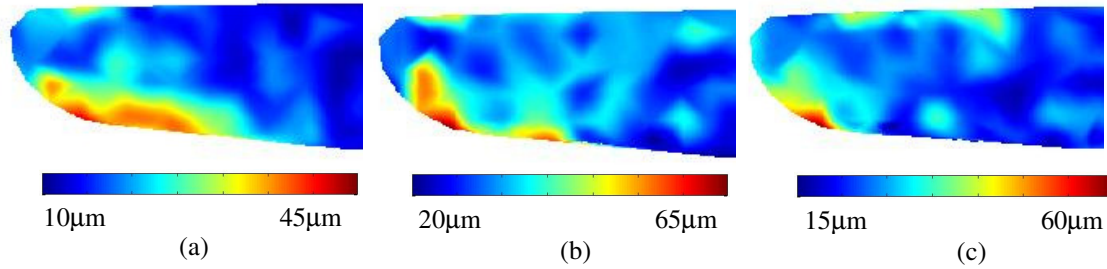
10μm   45μm   20μm   65μm   15μm   60μm

(a)   (b)   (c)

Fig. 9 Examples of standard deviation from average deflected shapes of wing: (a) AoA -0.95^o, Speed 30 mph, (b) AoA 5.1^o, Speed 40 mph, (c) AoA 11.4^o, Speed 40 mph.

Fig. 8 and Fig. 9 also demonstrate the limitation of videogrammetry measurements in wind tunnel testing. Accurate measurements require deflection to be visible to the cameras, meaning any motion less than a pixel is unresolvable. The Nighthawk's wingspan is 66 cm, and the collected images were 1280 x 1024 pixels, yielding a camera resolution of approximately 0.5 mm/pixel. This resolution correlates to the maximum error of 0.62 mm measured in the calibration tests discussed previously. The average deflected shapes shown in Fig. 8 on the order of several centimeters are well above the noise floor of the videogrammetry measurement and correspondingly appear smooth. The standard deviations of the vibration amplitude from the average deflected shapes in Fig. 9 are on the order of tens of microns, below the noise floor of the videogrammetry measurement. Correspondingly these figures appear quite noisy, resulting in a lack of confidence in the results. While the resolution limits of the cameras may minimize the usefulness of videogrammetry in standard rigid-wing wind tunnel testing, their unique ability to capture large amplitude motion well above the maximum threshold of laser measurement systems makes them well-suited to these types of flexible-wing MAV measurements.

Power spectral densities of four points on the wing for the same case as in Fig. 7, the -0.95^o AoA, 30 mph wind speed case, are shown in Fig. 10. Also shown are the targets on the wing corresponding to the plotted PSD's. Fig. 10 confirms a resonance frequency in the *x* and *z* directions around 31 Hz.

Examination of other AoA and wind speed cases in Fig. 11 and Fig. 12 demonstrates the capability of this videogrammetry method to characterize both large deflections on the order of centimeters and small deflections on the order of millimeters. Fig. 11 shows a much higher peak, over -20 dB in one case, corresponding to much higher amplitude deflection in the wing than in the previous figure. Fig. 12 shows a case in which, while some highly-damped resonance is indicated in the *y*-direction by the wide peak at 22.5 Hz, the motion is of such low amplitude that it is extremely difficult to visualize. In this case it appears that either resonance motion does not occur, which would indicate that the wing does not experience flutter under these test conditions, it occurs at amplitudes below the resolution of the videogrammetry measurement, or it occurs at a frequencies above the measurement bandwidth of half the frame rate or 37.5 Hz in this case. Note that higher frame rate cameras can be used to expand the dynamic range of measurement.
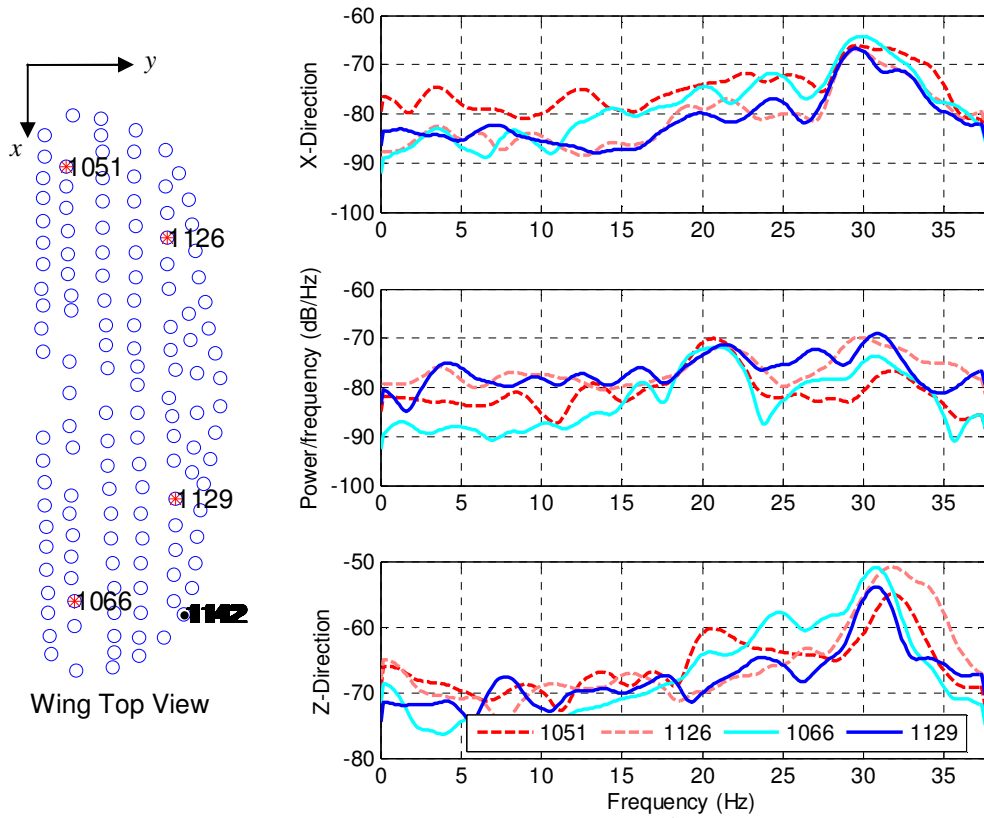
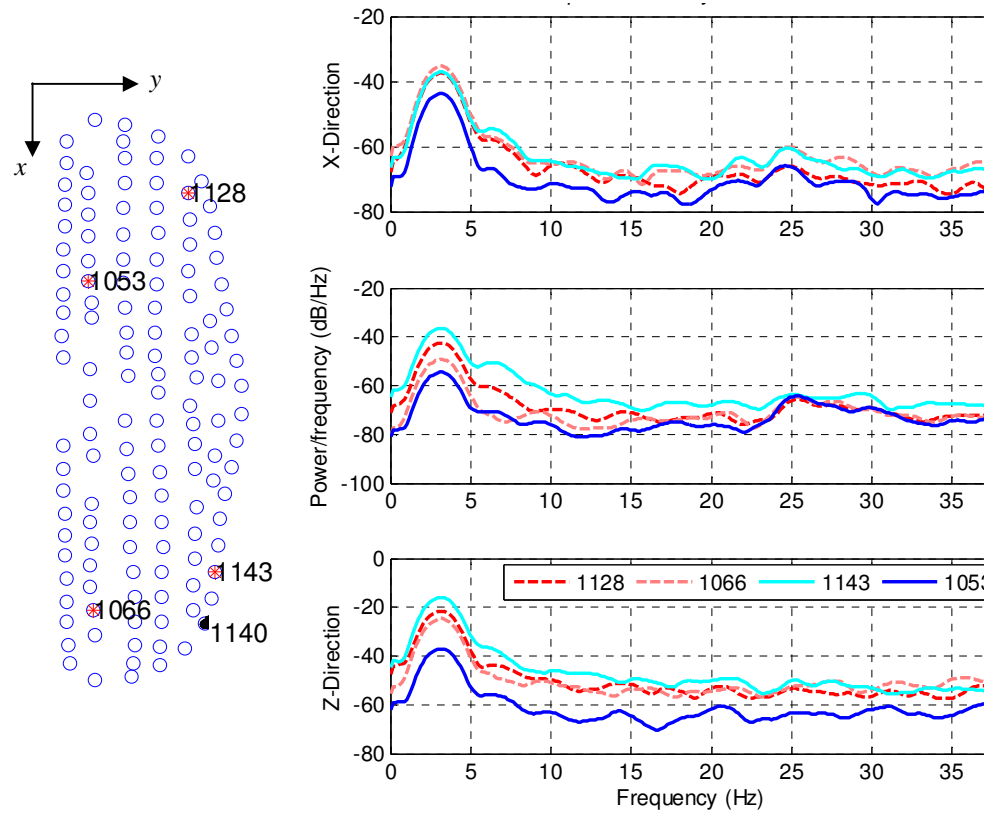American Institute of Aeronautics and Astronautics

Fig. 10 Power Spectral Densities of multiple points for AoA -0.95°, Speed 30 mph, *x, y, z*-directions.

Fig. 11 Power Spectral Densities of multiple points for AoA -0.95°, Speed 40 mph *x, y, z*-directions.

10
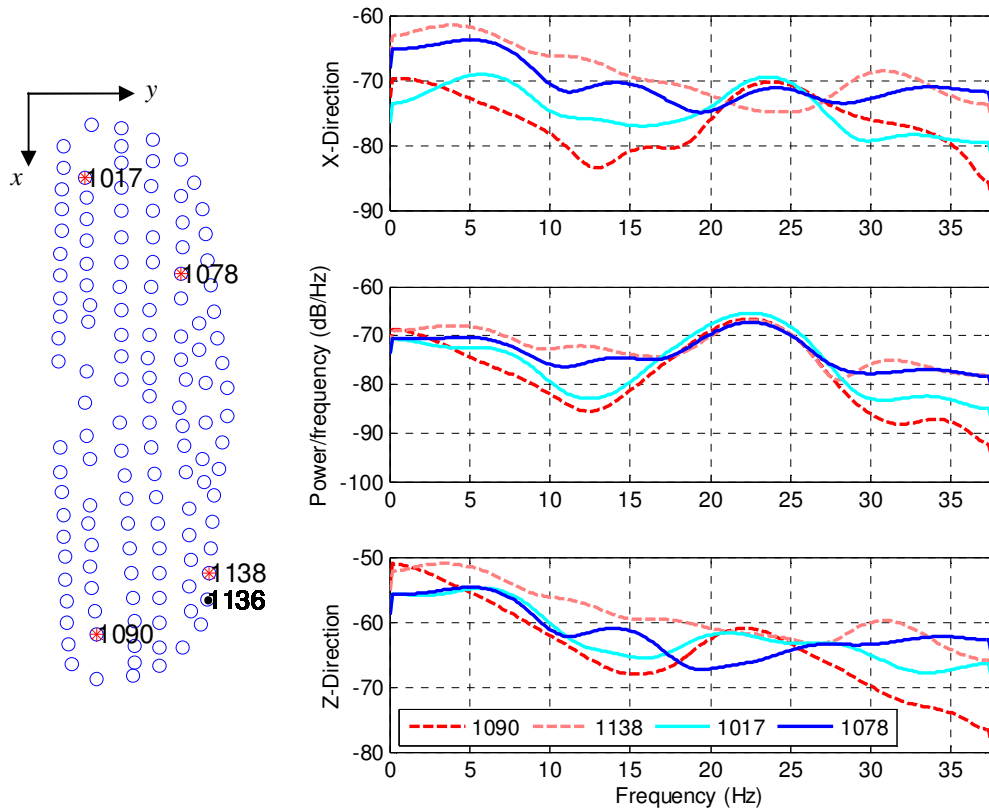American Institute of Aeronautics and Astronautics

Fig. 12 Power Spectral Densities of multiple points for AoA 13.4^o, Speed 20 mph, *x, y, z*-directions.

Further examination of Fig. 10 – Fig. 12 shows several instances in which peaks occur at the same frequencies in multiple directions. The best example is Fig. 11, in which there is clearly resonance in all three directions at 3.2 Hz. In the AoA -0.95^o, 30 mph case in Fig. 10 peaks occur in the *x* and *z*-directions at 29.5 Hz. Assuming that the peaks correspond to the first bending or first torsion mode of the wing, both in and out-of-plane motion is expected in *x* and *z*, while significantly less is expected in the *y*-direction. *y*-direction only resonance is expected for rigid body rocking of the test article and fixture. Based on the directional coupling of peaks in the PSD's, suppositions can be made regarding the corresponding deflection shape, but another advantage of this videogrammetry technique is that it also enables shape visualization.

An important contribution of this technique is the capability to visualize the ODS corresponding to peaks in the frequency domain as seen in the graphs in Fig. 10 and Fig. 11 by temporally filtering the time histories of the measured 3D points, fitting a surface to those points at each time step (frame), and animating the surface. Animating the ODS is a powerful tool that shows scaled asymmetric flapping or flutter behavior in Fig. 13 (a) and (b) corresponding to the resonance peak at 3.2 Hz in the AoA -0.95^o, Speed 40 mph case. In addition to large-amplitude motion, the technique allows visualization of small-amplitude in-plane rippling of the AoA 3.2^o, Speed 40 mph case shown in Fig. 13 (c).
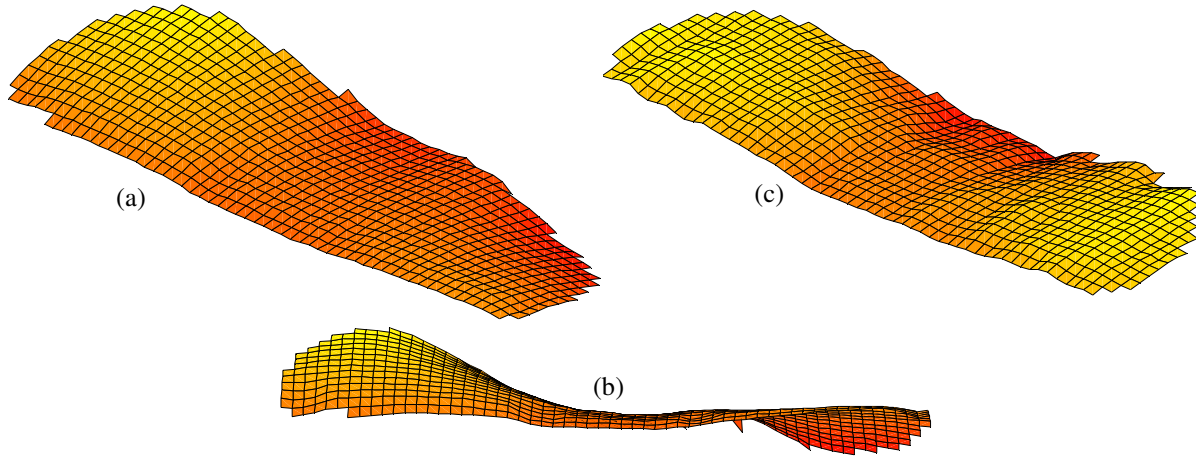
American Institute of Aeronautics and Astronautics

Fig. 13 Frames of animated deflection shapes of wing: (a) 3D pictorial view of AoA -0.95°, Speed 40 mph at 3.2 Hz, (b) front view of AoA -0.95°, Speed 40 mph at 3.2 Hz, (c) 3D pictorial view of AoA 3.2°, Speed 40 mph no filter.

Summaries of the results of the visualization of the ODS corresponding to peaks in the PSD's of all test cases are listed in Table 2. Analysis shows that the flexible Nighthawk wing that was tested is susceptible to flapping or flutter at low and high angles of attack. In this case flutter is considered to be a coupling between the first bending and first torsion modes of the wing. This behavior was clearly visible in the -0.95° AoA, 30 mph case. The cases classified as asymmetric flapping, shown in Fig. 13 (a) and (b), appear only to have the asymmetric torsion component, and are therefore not classified as flutter. Both conditions are dynamic instabilities experiencing unbounded amplitude increases that structural damping is insufficient to prevent, resulting in loss of stability. At the mid-range AoA's between 1.15° and 11.4°, the only apparent spectral content in the measured response of the wing is a highly-damped rigid body rocking mode that is likely a result of the fixing of the test article on a sting in the flow. The characterization of ODS's as presented here is a critical component in the validation of numerical models and simulations, and the design, optimization, and control of lightweight flexible aerospace structures.

Table 2 also shows the measured maximum wing deflection from the average deflected shape (Fig. 8) for each of the test cases. These results are plotted in Fig. 14. This graph clearly demonstrates that at 20 mph, the wings experience very low vibration amplitudes at any of the measured AoAs indicating that there should be little chance of flutter or other instabilities. This conclusion is supported by the data in Table 2 which shows only a couple of cases in which any spectral content was visible at 20 mph. Also confirming results from Table 2, Fig. 14 shows that at low AoAs, substantial motion was recorded for the 30 and 40 mph cases. A slight increase in deflection is also visible at the 13.4° AoA. Fig. 10 – Fig. 12 show the location on the wing at which the maximum deflection from the average deflected shape occurred, indicated by the solid markers. As expected, in all cases the maximum deflection occurred at the trailing edge of the wing, away from both the rigid leading edge and aircraft body. These results indicate that the Nighthawk wing should be stable in most flight regimes with the exception of high-speed, low AoA cases.

The maximum wing deflection from average deflected shape values reported in Table 2 help to clarify the accuracy of the videogrammetry measurements. In most cases in which the ODS is inconclusive there is a small maximum deflection, less than 0.5 mm. The clearest ODS's occurred in test cases in which the maximum deflection of the wing was greater than 0.5 mm. This conclusion coincides with the camera pixel resolution threshold discussed previously; resulting in high confidence in the resonance frequencies and corresponding ODS extracted through this extension of videogrammetry.

Unconventional data such as wing damping may also be extracted spectrally from the videogrammetry data through the half-power or other method,[21] and the technique can also measure in-plane and out-of-plane strains.

Table 2 Test Results

| AoA (deg)	Speed (mph)	Resonance Frequency (Hz)	ODS Comments	Max Deflection z-dir (cm)
-5.05	21.1	not visible	n/a	0.08
	31.7	1.3	asymmetric flapping	1.50
	42.1	2.5	asymmetric flapping	3.44
-2.9	21.1	21.3	asymmetric flapping, noisy	0.03
	31.8	2.6	asymmetric flapping	0.95
	42.4	2.6	asymmetric flapping	2.53
-0.95	21.4	not visible	n/a	0.04
	31.9	29.5	flutter	0.11
	42.4	3.2	asymmetric flapping	1.07
1.15	21.1	not visible	n/a	0.03
	31.8	29.3	possible rigid body rocking	0.04
	42.6	22.0	possible rigid body rocking	0.10
3.2	21.1	not visible	n/a	0.04
	31.9	29.6	possible rigid body rocking	0.04
	42.7	21.5	possible rigid body rocking	0.05
5.1	21.7	not visible	n/a	0.01
	32.3	16.5, 28.9	possible rigid body rocking	0.02
	43.1	21.5	possible rigid body rocking	0.05
7.3	21.1	22.0	possible rigid body rocking	0.02
	31.8	not visible	n/a	0.03
	42.1	21.5	possible rigid body rocking	0.05
9.4	21.5	21.7, 27.8	possible rigid body rocking	0.03
	32.2	21.7, 29.5	rigid body rocking at 21.7	0.02
	42.1	21.7	possible rigid body rocking	0.04
11.4	21.4	22.3	rigid body rocking, noisy	0.02
	31.6	29.6	rigid body rocking, noisy	0.04
	42.3	22.0	possible rigid body rocking	0.05
13.4	21.4	22.5	rocking / flapping	0.06
	31.5	22.0	rocking / flapping	0.08
	42.1	24.6	rocking / flapping	0.15
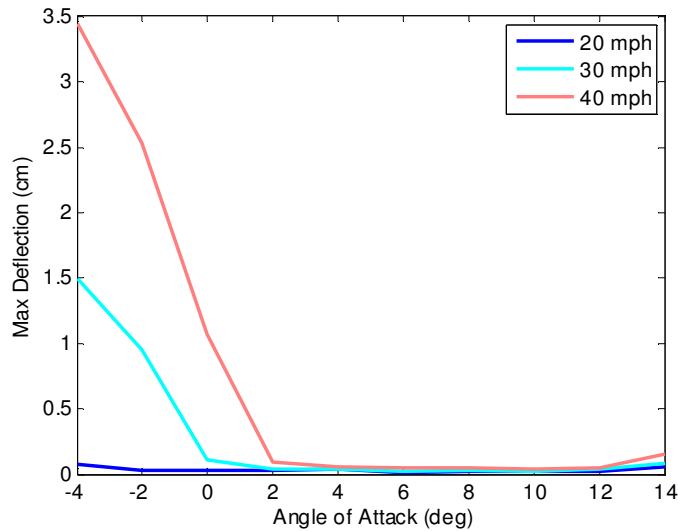
Fig. 14 Plots of maximum recorded deflection vs. angle of attack.

IV. Conclusions

The presented work uses non-contact videogrammetry measurement techniques to analyze flexible, lightweight carbon fiber composite mini-UAV wings in wind tunnel testing. These flexible wings are of interest due to their stability in flight and low mass. The wind tunnel data here shows the wing to be very stable at all tested wind speeds, up to 40 mph, for AoA's greater than 0°. The wing only exhibited flutter/flapping behavior at negative AoA's corresponding to low C_L. The flexible nature of the wing was evident in the large deflections of over 3.4 cm it experienced during flutter.

The videogrammetry technique used here extends previous measurements to capture the resonance frequencies and corresponding operating deflection shapes of the wings over the measured range of AoA's and wind speeds. This technique allowed the observed unstable flutter behavior was distinguished from rigid body rocking of the test fixture. The knowledge of the deflection shape of the wing at different resonance frequencies is necessary to understand the complicated membrane-structure interactions as MAV's become smaller and lighter, and to validate structural, aeroelastic, and aerodynamic numerical models, optimize wing aerodynamic performance as a function of angle of attack, Reynolds number, and geometry, and control flutter. The presented data show that videogrammetry will play a key role in the development of future lightweight MAV systems.

Acknowledgments

References

[1]Burner, A. W. and Liu, T., "Videogrammetric Model Deformation Measurement Technique," *Journal of Aircraft*, Vol. 38, No. 4, 2001, pp. 745-754.

[2]Barrows, D. A., "Videogrammetric Model Deformation Measurement Technique for Wind Tunnel Applications," 45th AIAA Aerospace Sciences Meeting and Exhibit, Reno, NV, Jan. 2007, AIAA Paper 2007-1163.

[3]Simpson, A., Rowe, J., Smith, S., and Jacob, J., "Aeroelastic Deformation and Buckling of Inflatable Wings under Dynamic Loads," 48th AIAA/ASME/ASCE/AHS/ASC Structures, Structural Dynamics, and Materials Conference, Honolulu, HI, Apr. 2007, AIAA Paper 2007-2239.

[4]Graves, S. S., Burner, A. W., Edwards, J. W., and Schuster, D. M., "Dynamic Deformation Measurements of an Aeroelastic Semispan Model," *Journal of Aircraft*, Vol. 40, No. 5, 2003, pp. 977-984.

[5]Albertani, R., Stanford, B., Hubner, J. P., and P. G. Ifju, "Aerodynamic Coefficients and Deformation Measurements on Flexible Micro Air Vehicle Wings," *Journal of Experimental Mechanics*, Vol. 47, No. 5, 2007, pp. 625–635, doi: 10.1007/s11340-006-9025-5

[6]Meyn, L., and Bennett, M.S., "A Two Camera Video Imaging System with Application to Parafoil Angle of Attack Measurements," 29th Aerospace Sciences Meeting, Reno, NV, Jan. 1991, AIAA Paper 91-0673.

[7]Fleming, G. A., Bartram, S. M., Waszak, M. R., and Jenkins, L. N., "Projection Moiré Interferometry Measurements of Micro Air Vehicle Wings", SPIE International Symposium on Optical Science and Technology, San Diego, CA, July 2001, SPIE Paper No. 4448-16.

[8]Black, J. T., Smith, S. W., Leifer, J., and Bradford, L., "Measuring and Modeling the Dynamics of Stiffened Thin Film Polyimide Panels," *Journal of Guidance, Control, and Dynamics*, Vol. 31, No. 3, 2008, pp. 490–500. doi:10.2514/1.32236

[9]Pappa, R. S., Black, J. T., Blandino, J. R., Jones, T. W., Danehy, P. M., and Dorrington, A. A., "Dot Projection Photogrammetry and Videogrammetry of Gossamer Space Structures," *Journal of Spacecraft and Rockets*, Vol. 40, No. 6, 2003, pp. 858–867. doi:10.2514/2.7047

[10]Flint, E., Bales, G., Glaese, R., and Bradford, R., "Experimentally Characterizing the Dynamics of 0.5 m Diameter Doubly Curved Shells Made From Thin Films," AIAA Paper 2003-1831, April 2003.

[11]Pitcher, N.A., and R.C. Maple, "A Static Aeroelastic Analysis of a Flexible Wing Mini Unmanned Aerial Vehicle," 38th AIAA Fluid Dynamics Conference and Exhibit, Seattle, WA, June 2008, AIAA Paper 2008-4057.

[12]Pitcher, N. A., "A Static Aeroelastic Analysis of a Flexible Wing Mini Unmanned Aerial Vehicle," Master's thesis, Department of Aeronautics and Astronautics, Air Force Institute of Technology, March 2008.

[13]Stults, J., Maple, R., Cobb, R., and Parker, G., "Computational Aeroelastic Analysis of Micro Air Vehicle with Experimentally Determined Modes," 23rd AIAA Applied Aerodynamics Conference, Toronto, Ontario, June 2005, AIAA Paper 2005-4614.

[14]Ifju, P., Jenkins, D. A., Ettinger, S., Lian, Y., Shyy, W., and Waszak, M. R., "Flexible-Wing-Based Micro Air Vehicles." 40th AIAA Aerospace Sciences Meeting & Exhibit, Jan. 2002, AIAA Paper 2002-0705.

[15]Shyy, W., Klevebring, F., Nilsson, M., Sloan, J., Carroll, B., and Fuentes, C., "Rigid and Flexible Low Reynolds Number Airfoils," *Journal of Aircraft*, Vol. 36, No. 3, 1999, pp. 523–529.

[16]DeLuca, A. M., Reeder, M. F., Freeman J., and Ol, M. V., "Flexible- and Rigid-Wing Micro Air Vehicle: Lift and Drag Comparison," *Journal of Aircraft*, Vol. 43, No. 2, 2006, pp. 572-575.

[17]Wong, K. W., "Basic Mathematics of Photogrammetry," Chapter 2, *Manual of Photogrammetry*, 4th Edition, Slama, C.C., ed., American Society of Photogrammetry, Falls Church, Virginia, pp. 37-101, 1980.

[18]Mikhail, E.M., Bethel, J.S., and J.C. McGlone, Introduction to Modern Photogrammetry, John Wiley & Sons, New York, NY, ISBN 0471309249, 2001.

[19]Atkinson, K.B., ed., Close Range Photogrammetry and Machine Vision, Whittles Publishing, Caithness, Scotland, ISBN 1870325737, 2001.

[20]Eos Systems Inc., *PhotoModeler 6 User Guide*, 1st Ed., Jan. 2007.

[21]Inman, D.J., *Vibration with Control, Measurement, and Stability*, Prentice Hall, New Jersey, ISBN 0139427988, 1989.